# The effect of hierarchical single-crystal ZSM-5 zeolites with different Si/Al ratios on its pore structure and catalytic performance

Hou, Yuexin; Li, Xiaoyun; Sun, Minghui; Li, Chaofan; Bakhtiar, Syed ul Hasnain; Lei, Kunhao; Yu, Shen; Wang, Zhao; Hu, Zhiyi; Chen, Lihua; Su, Bao Lian

*Published in:*
Frontiers of Chemical Science and Engineering

*DOI:*
10.1007/s11705-020-1948-3

*Publication date:*
2021

*Document Version*
Publisher's PDF, also known as Version of record

Front. Chem. Sci. Eng.
https://doi.org/10.1007/s11705-020-1948-3

RESEARCH ARTICLE

# The effect of hierarchical single-crystal ZSM-5 zeolites with different Si/Al ratios on its pore structure and catalytic performance

**Yuexin Hou[1*], Xiaoyun Li[2*], Minghui Sun[1,3], Chaofan Li[1,4], Syed ul Hasnain Bakhtiar[1], Kunhao Lei[1], Shen Yu[1], Zhao Wang[1], Zhiyi Hu[1,4], Lihua Chen (✉)[1], Bao-Lian Su (✉)[1,3,5]**

1 Laboratory of Living Materials at the State Key Laboratory of Advanced Technology for Materials Synthesis and Processing, Wuhan University of Technology, Wuhan 430070, China
2 State Key Laboratory of Silicate Material for Architectures, Wuhan University of Technology, Wuhan 430070, China
3 Laboratory of Inorganic Materials Chemistry (CMI), University of Namur, B-5000 Namur, Belgium
4 Nanostructure Research Centre (NRC), Wuhan University of Technology, Wuhan 430070, China
5 Clare Hall, University of Cambridge, Cambridge, CB3 9AL, UK



**Abstract** Hierarchical single-crystal ZSM-5 zeolites with different Si/Al ratios (Hier-ZSM-5-*x*, where $x$ = 50, 100, 150 and 200) were synthesized using an ordered mesoporous carbon-silica composite as hard template. Hier-ZSM-5-*x* exhibits improved mass transport properties, excellent mechanical and hydrothermal stability, and higher catalytic activity than commercial bulk zeolites in the benzyl alcohol self-etherification reaction. Results show that a decrease in the Si/Al ratio in hierarchical single-crystal ZSM-5 zeolites leads to a significant increase in the acidity and the density of micropores, which increases the final catalytic conversion. The effect of porous hierarchy on the diffusion of active sites and the final catalytic activity was also studied by comparing the catalytic conversion after selectively designed poisoned acid sites. These poisoned Hier-ZSM-5-*x* shows much higher catalytic conversion than the poisoned commercial ZSM-5 zeolite, which indicates that the numerous intracrystalline mesopores significantly reduce the diffusion path of the reactant, leading to the faster diffusion inside the zeolite to contact with the acid sites in the micropores predominating in ZSM-5 zeolites. This study can be extended to develop a series of hierarchical single-crystal zeolites with expected catalytic performance.

Received February 19, 2020; accepted April 15, 2020

E-mails: chenlihua@whut.edu.cn (Chen L),
bao-lian.su@unamur.be (Su B-L)

* These authors contributed equally to this work.

**Keywords** hierarchical zeolites, single crystalline, interconnected pores, improved diffusion performance, benzyl alcohol self-etherification reaction

## 1 Introduction

Natural evolution has produced optimized hierarchically structured organisms in both plant and animal form in which the pore size decreases regularly and finally terminates in size-invariant units [1,2]. Such well-designed hierarchically porous structures maximize mass-transfer and minimize energy-consumption [3,4]. In 1926, the Murray's law was proposed as a physical principle to explain the optimized hierarchical design in natural biological respiratory and circulatory systems [5]. However, Murray's law in its original form is not applicable in the fields of synthetic materials because of the difficulties in constructing vascularized structures. A breakthrough was achieved by our group when we extended Murray's law to design hierarchically structured inorganic materials [6]. Mimicking nature's hierarchical networks, each level of porosity in these synthetic Murray materials was integrated in a hierarchical manner to significantly improve the structure and thereby gain the full benefits in catalytic performance [6]. Crystalline microporous zeolites are widely used inorganic solid acid catalysts in petroleum and chemical industries due to their well-defined microporous structure [7–10]. However, the very existence of these small micropores usually imposes severe diffusion constraints for bulky molecules that diffuse in and out of the reactive sites within the pore system [11,12]. Two

fundamentally different strategies were adopted to solve such diffusion limitations: (1) decreasing the crystalline size and (2) introducing the additional pore system into an individual zeolite crystal [13–18]. Both methods offer an effective solution to achieve a faster mass transfer in the zeolites, thus decreasing the possible conversion of reactants into unwanted side products in addition to boosting the catalytic performance. However, following the decrease of the crystalline size, the low crystallinity and the aggregation of zeolite nanocrystals limit their applications. Thus, zeolites with the intracrystalline hierarchically porous structure have gained increasing interest. More importantly, the additional porosity should be introduced into zeolites without decreasing micropore density, thus ensuring better molecular sieving of hierarchically porous zeolites [19].

Numerous studies have reported the synthesis of hierarchical porous zeolites generally by using template methods (soft-template and hard-template method) [20–24] and post-processing methods (dealumination or desilication) [25–28]. However, etching through dealumination or desilication damages the zeolite framework structure [29–31]. Furthermore, the surfactants required by the soft-template method also incur limitations due to their complex nature and high cost [32,33]. The hard-template method is not only simple and efficient but also preserves the framework structure of zeolites [34]. Notably, the hard-template method was proven to create ordered mesoporous structures and precisely control mesopore size. Wang et al. [35] applied three-dimensionally ordered mesoporous carbon (20, 40 and 80 nm) as a template to obtain hierarchical SAPO-34 zeolites with a three-dimensionally ordered mesoporous-imprinted structure, and the ordered mesopore size could be tuned from 5.5 to 13.0 nm by varying the size of the three-dimensionally ordered carbon (from 20 to 80 nm). Based on the generalized Murray's law on the design of suitable pore size, our group designed an *in-situ* crystallization approach for constructing hierarchical single-crystal MFI zeolites by using ordered mesoporous carbon-silica composite as a hard template. The as-prepared hierarchical single-crystal ZSM-5 zeolites were fabricated from zeolite nanocrystals, which offer improved catalytic properties and higher stability in the cracking reaction of isopropyl benzene [36]. In addition to introducing mesopores into zeolite catalysts, the adjustable Si/Al ratio is also an indispensable factor to evaluate the physical and chemical properties of hierarchical single-crystal ZSM-5 zeolites. Considerable studies have controlled the Si/Al ratio in zeolites to investigate its catalytic capacity [37–39], but few studies have shown that the Si/Al ratio of ZSM-5 zeolites can affect catalytic performance by changing the acidity and the density of micropores present in the zeolite framework. The bare benzyl alcohol (BA) self-etherification reaction [40] was the optimal probe reaction, which is an important reaction in the production of pharmaceutical intermediates and fine chemicals and an environmentally friendly reaction with water as a by-product [41]. Note that 2,6-di-tert-butylpyridine (DTBP) may be added in another BA self-etherification reaction to poison the active sites on the surface of the zeolites, so that only the active sites inside the zeolitic micropores could contact the BA and participate in the reaction. The comparison of these reactions can be used to demonstrate the benefits of hierarchical single-crystal ZSM-5 zeolites and verify how the Si/Al ratio affects its catalytic performance.

Herein, we report the synthesis of hierarchical single-crystal ZSM-5 zeolites with different Si/Al ratios (Hier-ZSM-5-*x*, where $x$ = 50, 100, 150 and 200), in which we use an ordered mesoporous carbon-silica composite as hard template. Hierarchical single-crystal ZSM-5 zeolites are composed of numerous closely packed nanocrystals and nanorods with the same orientation, thus producing numerous intracrystalline mesopores. The results show that hierarchical single-crystal ZSM-5 zeolites offer excellent mechanical and hydrothermal stability. In addition, because introducing more aluminum into the zeolitic framework forms more micropores by increasing the number of defects in the framework and more active sites, the decrease of the Si/Al ratio significantly increases the acidity and the micropore density present in the zeolite framework. We choose the BA self-etherification reaction as probe reaction, and the hierarchical single-crystal ZSM-5 zeolites offer better catalytic performance than commercial ZSM-5 zeolites (Com-ZSM-5). In another study, the external active sites were poisoned by DTBP and the hierarchical single-crystal ZSM-5 zeolites still exhibited higher catalytic performance as compared with Com-ZSM-5. This improved catalytic performance is further explained by the introduction of mesopores, which greatly reduce the diffusion path so that reactants and products can more easily diffuse in and out of the zeolitic framework *vis-à-vis* Com-ZSM-5, which have only micropore present in the framework. We further explored how the Si/Al ratio affects hierarchical single-crystal ZSM-5 zeolites, and the increased catalytic performance in the BA self-etherification reaction with decreasing Si/Al ratio. The main reason for this increase is that a decreased Si/Al ratio renders hierarchical single-crystal ZSM-5 zeolites more acidic and increases the density of micropores, allowing the use of more acid sites in the microporous framework of ZSM-5 zeolite.

## 2 Experimental

### 2.1 Materials

We used the following reagents without further purification: polyethylene oxide-polypropylene oxide-polyethylene oxide (P123, Sigma-Aldrich Co., Ltd.), sodium dodecyl sulfate (SDS, Sinopharm Chemical

Reagent Co., Ltd.), tris(hydroxymethyl) methyl aminomethane (TMA, Aladdin Chemistry Co., Ltd.), LUDOX® AS-40 colloidal silica (40 wt-% suspension in $H_2O$, Sigma-Aldrich Co., Ltd.), dopamine hydrochloride (Xiya Reagent Co., Ltd.), tetrapropylammonium hydroxide (TPAOH, 1 mol·L$^{-1}$, Aladdin Chemistry Co., Ltd.), aluminum isopropoxide ($C_9H_{21}AlO_3$, Aladdin Chemistry Co., Ltd.), and Com-ZSM-5 (Sinopharm Chemical Reagent Co., Ltd.).

### 2.2 Synthesis of silica spheres coated with mesoporous carbon ($SiO_2$@PC)

Amorphous $SiO_2$ spheres with a mesoporous carbon coating were prepared by coprecipitation. Typically, 2 g P123 with 0.1 g SDS were first added to 200 mL deionized water at room temperature and stirred for 1 to 2 h until completely dissolved. Next, 3.15 g LUDOX® AS-40 colloidal silica was added dropwise to the gel and ultrasonically agitated for 30 min. The mixture was stirred continuously overnight followed by the addition of 1.2 g TMA and 2 g dopamine hydrochloride. The product was centrifuged more than three times and dried at 60 °C for at least 1 d. Finally, the solid was heated at 5 °C·min$^{-1}$ to carbonize at 800 °C for 2 h in an argon atmosphere. The resulting sample is denoted by $SiO_2$@PC.

### 2.3 Synthesis of Hier-ZSM-5-*x*

Based on our previous work, *in-situ* crystallization and steam assisted crystallization method were used herein to crystallize hierarchical zeolites [36]. The molar compositions of the hierarchical ZSM-5 were set to *y* $SiO_2$:1 $Al_2O_3$:23.3 TPAOH:1053 $H_2O$ (*y* = 100, 200, 300 and 400). In a typical synthesis, 7.25 g TPAOH and 0.0625 g $C_9H_{21}AlO_3$ were mixed in to form a homogeneous gel, which was then stirred for 1 h (the mixed gel served as precursor). Next, the $SiO_2$@PC was impregnated into a certain amount of precursor and dried at 40 °C for 1 d. The resultant product was transferred to a Teflon-lined stainless-steel autoclave with 5 mL $H_2O$ in the bottom at 180 °C for 12 h. The as-synthesized products were centrifuged, washed by deionized water, dried at 60 °C overnight and finally calcined at 550 °C for 7 h. The as-synthesized samples are denoted as Hier-ZSM-5-*x*. For the hydrothermal treatment of Hier-ZSM-5-100 in gas phase, 100 mg samples was placed in quartz tube and heated to 700 °C under nitrogen atmosphere, then, nitrogen gas was turned off and 100% vapor was passed and kept for 2 h, finally the sample was purged with nitrogen to room temperature. For the hydrothermal treatment of Hier-ZSM-5-100 in liquid phase, 100 mg samples were heated at 120 °C for 2 d in Teflon-lined stainless-steel autoclave. Finally, all samples that underwent hydrothermal treatment were calcined at 550 °C for 6 h.

### 2.4 Characterization

X-ray powder diffraction (XRD) patterns were recorded by using a Bruker D8 X-ray diffractometer with Cu-Kα radiation ($\lambda$ = 1.54056 Å, 40 kV and 40 mA). Scanning electron microscopy (SEM) images were collected by using a Hitachi S-4800 electron microscope. The samples were first degassed at 100°C for 12 h in quartz tubes and the $N_2$ adsorption-desorption isotherms were measured at −196°C by using a Micromeritics ASAP 2020 and Tristar system. The pore-size distribution was derived from the desorption peak of the isotherm based on the Barett-Joyner-Halenda model. $^{27}$Al and $^{29}$Si magic angle spinning nuclear magnetic resonance (MAS NMR) spectra were recorded by using a Bruker AVANCEIII HD 400 MHz spectrometer. High-angle annular dark field scanning transmission electron microscopy (HAADF-STEM), transmission electron microscopy (TEM), selected Area electron diffraction (SAED) and energy dispersive x-ray spectroscopy (EDX) were done by using a Thermo Fisher Talos microscope fitted with a Super-X EDX system, operated at 200 kV. The sample components were analyzed by using an inductively coupled plasma (ICP) with a Perkin Elmer Optima 5300DV emission spectrometer. The $NH_3$-temperature programmed desorption ($NH_3$-TPD) was measured by using AutoChem II 2920, 100 mg ZSM-5 zeolites were first purged with helium at 550 °C for 30 min, then cooled to room temperature and allowed to adsorb ammonia for 30 min. The signal was collected by using thermal conductivity detector at a rate of 10 °C·min$^{-1}$ from 100 °C to 550 °C. The Fourier transform infrared (FTIR) data was collected by using a Nicolet 6700 FTIR spectrometer equipped with an MCT detector in the region of 4000–400 cm$^{-1}$. The X-ray photoelectron spectroscopy (XPS) was done by using a Thermo Scientific Kα XPS spectrometer equipped with a monochromatic Al-Kα x-ray source. X-ray fluorescence (XRF) was recorded by using a LAB CENTER XRF-1800.

### 2.5 Catalytic reaction

Hierarchical single-crystal ZSM-5 zeolites underwent ion exchange for three times. The samples were placed in 1 mol·L$^{-1}$ $NH_4NO_3$ solution and stirred at 80 °C for 3 h and then calcined at 550 °C for 6 h. The catalytic performance of synthesized hierarchical ZSM-5 zeolites was tested by using a BA self-etherification reaction. The specific experimental protocol for this catalytic reaction is described by Zhang et al. [40]. For this reaction, 15 mL 1,3,5-trimethylbenzene was used as a solvent, and 0.117 g catalyst activated at 550 °C for 4 h was added to the solvent. The mixed solution was placed in a three-necked flask and stirred at 70 °C and 0.25 mL BA was added. The reaction time was 2.5 h after the addition of BA. Then

0.051 mL DTBP was added in another BA self-etherification reaction for poisoning the active sites on the outer surface of the zeolites. The reaction supernatant was extracted at regular intervals and analyzed by using an Agilent 7890B gas chromatograph equipped with a flame ionization detector.

## 3 Results and discussion

In this work, 20 nm $SiO_2$@PC were fabricated and used as silicon source and hard template for synthesizing hierarchical single-crystal ZSM-5 zeolites. The XRD pattern and SEM image of $SiO_2$@PC are shown in Figs. S1 and S2 (cf. Electronic Supplementary Material, ESM) respectively, indicating the amorphous phase of $SiO_2$@PC, with rough spherical morphology. Figure S3 (cf. ESM) shows the $N_2$ adsorption-desorption isotherm of $SiO_2$@PC, which indicates that the sample contained numerous mesopores with wide size distribution. The $SiO_2$@PC was impregnated into a precursor solution containing TPAOH and an aluminum source and hydrolyzed to form dry aluminosilicate gel, which was further crystallized *in situ* under the induction of TPAOH as an organic structure-directing agent into ZSM-5 zeolite nanoparticles by steam assisted crystallization. In addition, a small amount of Si–O fragments flowed out through the mesopores of the carbon layer and co-crystallized with the help of TPAOH to form the final hierarchical single-crystal ZSM-5 zeolites ($x$ = 50, 100, 150 and 200 is the Si/Al ratio). At the same time, the TPAOH in the precursor solution was also used as an alkali source and the amount of TPAOH varied with the aluminum source.

The XRD pattern shows that all the samples with different Si/Al ratios had five peaks at 7.96°, 8.82°, 23.27°, 23.97° and 24.43°, which are characteristic of MFI-type zeolites (Fig. 1(a)) [13]. No obvious amorphous peaks were observed, indicating the formation of highly crystalline ZSM-5 zeolites. The FTIR absorption spectra of samples in Fig. S4 (cf. ESM) reveal all featured signals of a MFI-type framework structure, with peaks at 450, 550, 800, 1100 and 1250 $cm^{-1}$ [42]. The peak intensity ratios from the FTIR spectra show that $I_{550}/I_{450} > 0.7$ in all samples, indicative of high crystallinity [43], which is consistent with the XRD patterns.

As can be seen from the SEM images in Figs. 2(a) and 2(b), Hier-ZSM-5-50 presents typical coffin-shaped MFI-type zeolites, with a 2 μm crystal size, consisting of numerous closely packed nanocrystals and nanorods. The TEM image (Fig. 3(b)) shows a close packing of nanocrystals and nanorods in one individual ZSM-5 zeolite. The corresponding SAED patterns (Figs. 3(a) and 3(c)) reveal that the whole ZSM-5 zeolite particle is a single crystal along the same [111] orientation on both

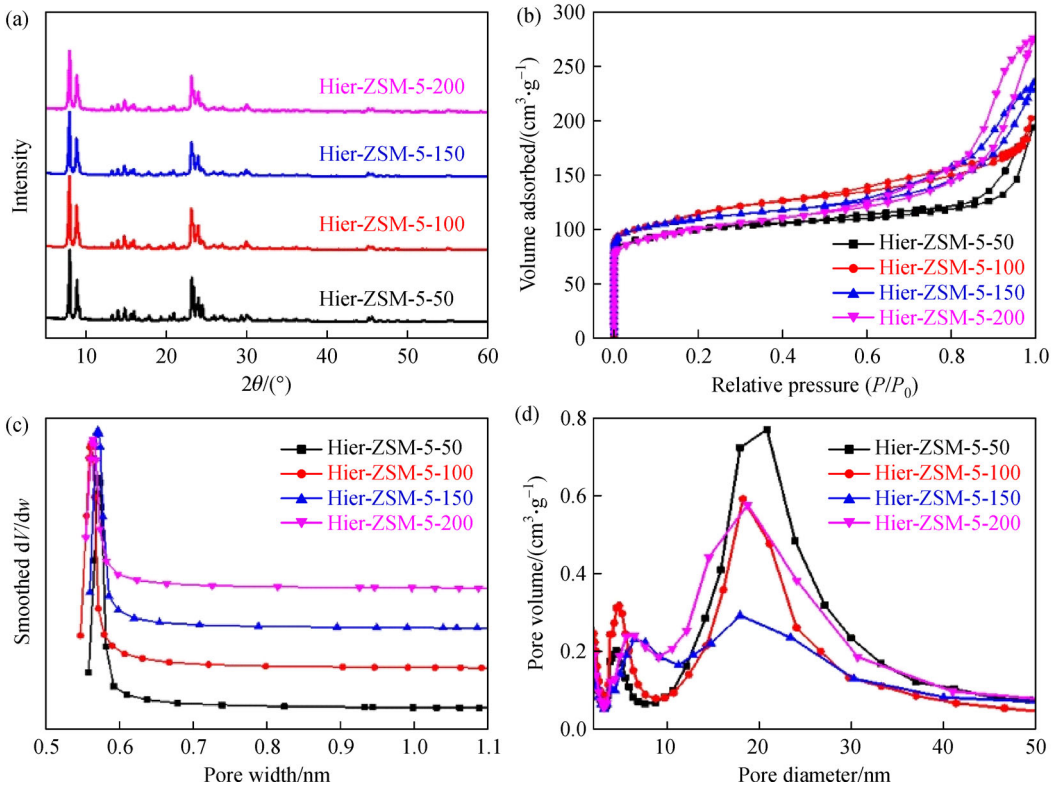


**Fig. 1** (a) XRD patterns; (b) nitrogen adsorption-desorption isotherms; (c) micropore size distributions; (d) mesopore size distributions of Hier-ZSM-5-*x*.

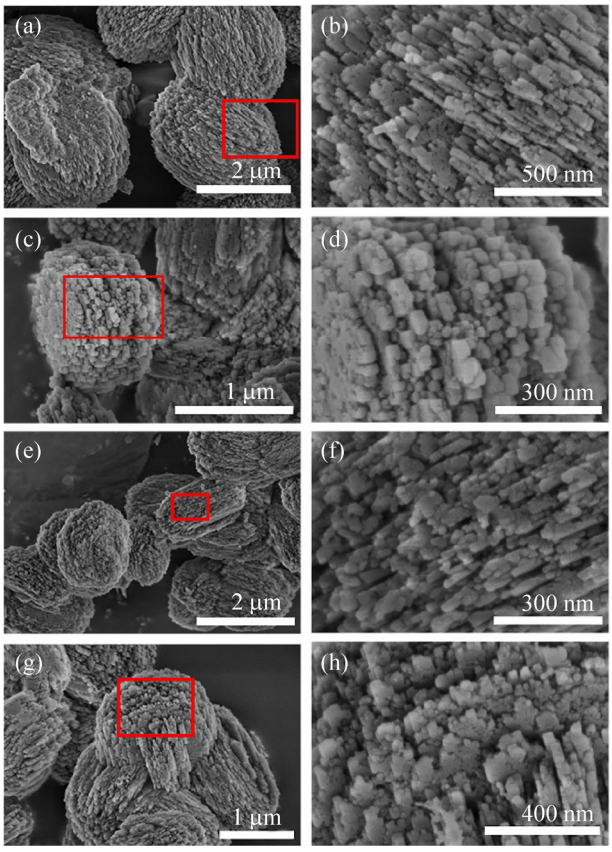


**Fig. 2** (a,b) SEM images of Hier-ZSM-5-50; (c,d) SEM images of Hier-ZSM-5-100; (e,f) SEM images of Hier-ZSM-5-150; (g,h) SEM images of Hier-ZSM-5-200.

sides of the particle. To gain more insight into the crystallographic structure, a high resolution transmission electron microscopy (HRTEM) image was used to investigate the fine structure of the ZSM-5 single crystal particle. Figures 3(d) and 3(e) and the corresponding fast Fourier transform (FFT) patterns (Figs. 3(f), insets of Figs. 3(d) and 3(e)) show the whole ZSM-5 zeolite crystal along the same zone axis again, the whole particle is composed of nanoparticles and nanorods, which are connected as a whole zeolite microporous crystal matrix. On the other side, the ZSM-5 zeolite presents a layered stack, as shown in the SEM image in Figs. 2(c) and 2(d). The TEM images and corresponding FFT pattern in Fig. S5 (cf. ESM) show that the nanorods and nanocrystals constituting the ZSM-5 zeolite are oriented along the same [101] axis and from a single crystal.

All the Hier-ZSM-5-*x* (Figs. 2(a–h)) present the same typical coffin-type morphology and crystal size (2 μm) as well. The rough outer surface of Hier-ZSM-5-*x* is formed by aggregation of small nanocrystals and nanorods. The morphology and crystal size of the zeolites clearly remain the same even with different Si/Al ratios, which indicates that these parameters are independent of the Si/Al ratio of the zeolite framework. We further investigated the distribution of Al atoms in zeolite single crystals. Figures S6 and S7 (cf. ESM) show HAADF-STEM images and corresponding EDX elemental maps of Hier-ZSM-5-100, respectively, where Fig. S6 is along [111] orientation and Fig. S7 is along [101] orientation. The Al atoms are distributed uniformly in the zeolite single crystal, and the Al and Si content is 0.48% and 44.22%, respectively, which is close to the Si/Al ratio (92) of the Hier-ZSM-5-100 sample.

$^{29}$Si MAS NMR and $^{27}$Al MAS NMR were used to investigate the chemical environments of the Si and Al framework in ZSM-5 zeolites. The silicon species in the ZSM-5 zeolite framework depends on the bond with which they attached, namely, $Q_4$[Si(OSi)$_4$] species, $Q_3$[Si(OSi)$_3$(OH) or Si(OSi)$_3$(Al)] species, and so on [44]. From Fig. 4(a), all samples exhibit only $Q_4$ (–110, –113, –116 ppm) and $Q_3$ (–102, –106 ppm) species [45]. The peak-intensity ratios of $Q_4/Q_3$ species were both exceed 20 and increased with increasing Si/Al ratio in all Hier-ZSM-5-*x* samples, indicating a high degree of condensation of the silicon species and an increasing in condensation with increasing Si/Al ratio. Combined with the previous XRD, SEM and TEM results, it shows that the samples are composed of ZSM-5 nanocrystals and nanorods with a high degree of condensation. Figure 4(b) shows $^{27}$Al MAS NMR of all ZSM-5 samples, the existence of resonance peaks at 53 ppm indicates that aluminum is only tetrahedrally coordinated in the framework of ZSM-5 zeolites, and no hexacoordinate (non-framework) aluminum appears in the samples [46,47]. The XPS spectra of aluminum (Fig. S8, cf. ESM) show that only the peaks of the framework aluminum appear in Hier-ZSM-5-*x* and the peak intensities of aluminum on the surface of the product decrease as the Si/Al ratio decreases. This result indicates that the initial feed aluminum introduced into the precursor easily forms tetracoordinate Al in ZSM-5 zeolites, with the help of SDAs, and the characteristic peak intensities of Al are closely related to the Si/Al ratio of the initial feed.

The physicochemical properties of Hier-ZSM-5-*x* are shown in Figs. 1(b–d) and Table 1. The $N_2$ adsorption-desorption isotherms (Fig. 1(b)) show that all samples present type-IV isotherms and type-$H_3$ hysteresis loops. The steep slope in the low relative pressure area ($P/P_0 < 0.01$) and the hysteresis loops for $0.6 < P/P_0 < 1.0$ confirm the existence of well-defined micropores and abundant mesopores in the samples. The micropore diameters are the same as conventional ZSM-5 zeolites (about 5.6 Å, see Fig. 1(c)), whereas the mesopore size distribution is centered at about 18 nm (Fig. 1(d)). The Brunner-Emmett-Teller (BET) surface areas of Hier-ZSM-5-*x* are 350, 376, 343 and 321 $m^2 \cdot g^{-1}$ (Table 1), respectively. The micropore surface areas of the Hier-ZSM-5-*x* samples are 266, 271, 213 and 161 $m^2 \cdot g^{-1}$, respectively. The BET surface areas and the micropore surface areas clearly decrease with the increasing Si/Al ratio. Note that the total pore volume (i.e., 0.28, 0.27, 0.36

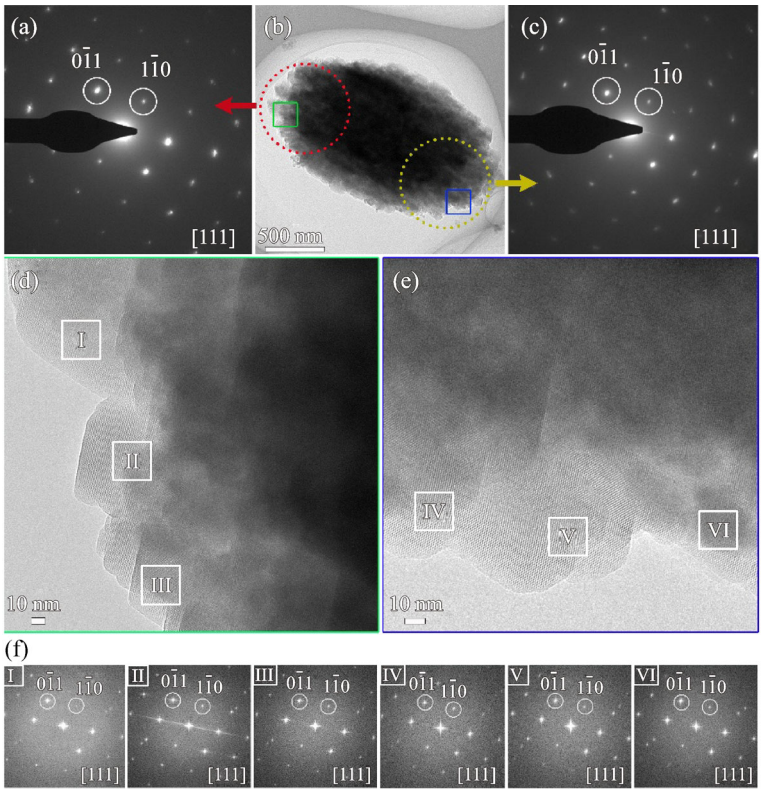


**Fig. 3** (b) TEM image of the Hier-ZSM-5-100 sample; (a,c) SAED patterns of the area indicated by the red and yellow dashed circles in panel (b), respectively; (d,e) HRTEM images of the area indicated by the green and blue boxes in panel (b), respectively; (f) FFT patterns of the area indicated by the white boxes in panel (d) and (e).

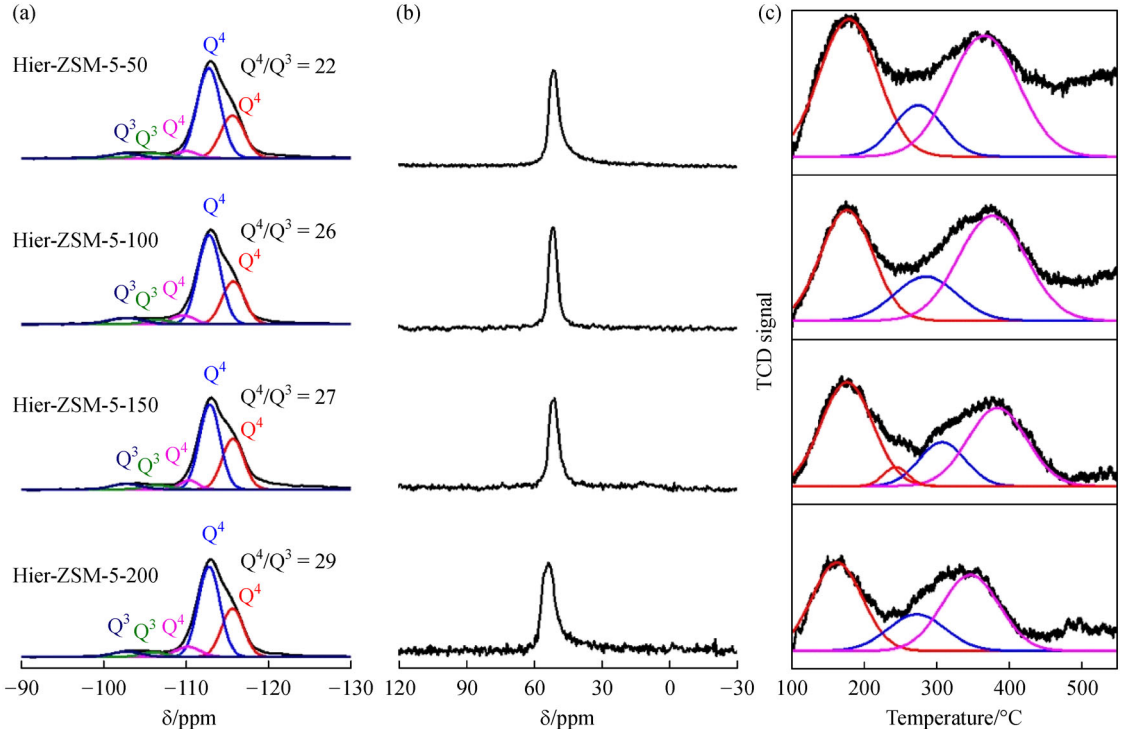


**Fig. 4** (a) $^{29}$Si MAS NMR spectra; (b) $^{27}$Al MAS NMR spectra; (c) $NH_3$-TPD profiles of Hier-ZSM-5-*x*.

**Table 1** Chemical and textural properties for samples and catalytic performance of ZSM-5 zeolite in BA self-etherification reaction

| Sample | $A_{BET}$ a) | $S_{micro}$ b) | $V_{total}$ c) | $V_{micro}$ d) | Si/Al e) | $X$(BA)/% | $S$(DBE)/% | $X$(BA)$^{\#}$/% | $S$(DBE)$^{\#}$/% |
|---|---|---|---|---|---|---|---|---|---|
| Hier-ZSM-5-50 | 350 | 266 | 0.28 | 0.14 | 64 | 93.8 | 96.1 | 88.4 | 96.6 |
| Hier-ZSM-5-100 | 376 | 271 | 0.27 | 0.14 | 128 | 86.3 | 96.3 | 79.8 | 96.0 |
| Hier-ZSM-5-150 | 343 | 213 | 0.36 | 0.11 | 170 | 84.2 | 94.2 | 64.1 | 90.3 |
| Hier-ZSM-5-200 | 321 | 161 | 0.42 | 0.08 | 235 | 81.7 | 93.8 | 61.6 | 87.5 |
| Com-ZSM-5 | 337 | 256 | 0.26 | 0.10 | 117 | 64.6 | 95.8 | 57.8 | 93.7 |

a) BET surface area of the samples by BET method ($m^2 \cdot g^{-1}$); b) micropore surface area of the samples ($m^2 \cdot g^{-1}$); c) single point adsorption total pore volume at $P/P_0$ = 0.99 ($cm^3 \cdot g^{-1}$); d) micropore volume by *t*-plot method ($cm^3 \cdot g^{-1}$); e) Si/Al ratio determined by ICP method. $X$(BA) represents the conversion of BA and $S$(DBE) represents the selectivity of dibenzyl ether (DBE) in BA self-etherification reaction without DTBP; $X$(BA)$^{\#}$ represents the conversion of BA and $S$(DBE)$^{\#}$ represents the selectivity of DBE in BA self-etherification reaction containing DTBP.

and 0.42 $cm^3 \cdot g^{-1}$) increases and the micropore volume (i.e., 0.14, 0.14, 0.11 and 0.08 $cm^3 \cdot g^{-1}$) decreases as the Si/Al ratio increases. These results are attributed to the introduction of more aluminum into the zeolitic framework, which means that more $Q_3$ species form and more defects in the zeolitic framework are generated. The defects caused by introducing aluminum in the framework form more pores with the size of micropore so that the density of micropores increases with decreasing Si/Al ratio.

The acidity of Hier-ZSM-5-*x* was investigated by using $NH_3$-TPD (Fig. 4(c)); all samples have two desorption peaks. The peaks at 100 °C–200 °C and 350 °C–450 °C correspond to the weak and strong acidic sites of ZSM-5 zeolites, respectively. Gaussian fits of these two peaks give the corresponding peaks of the weak, moderate, and strong acid sites [14], and the relative amount of acidity is compared by calculating the peak areas (Table S2 (cf. ESM)). The relative amount of acidity clearly increases with decreasing Si/Al ratio, which is attributed to the increased defect density in the framework caused by the introduction of more aluminum in the framework of ZSM-5 zeolites, which generates more acid sites.

To verify the mechanical stability of the ZSM-5 zeolites, Hier-ZSM-5-100 was crushed under a pressure of 50 MPa. The sample remained with well-defined MFI-type diffraction peaks, as confirmed by XRD (Fig. 5(a)), and the surface of the sample remained intact with no collapsed (Fig. 5(c-I). The physical and chemical properties of the sample were not disturbed. In addition, the hydrothermal stability of zeolites in both the liquid and gas phases was demonstrated. Figures 5(c-II) and 5(c-III) show that the morphology of the treated Hier-ZSM-5-100 samples is substantially unbroken. As can be seen from Fig. 5(b) and Table S1 (cf. ESM), the micropore surface area of Hier-ZSM-5-100 decreases slightly, indicating the partial

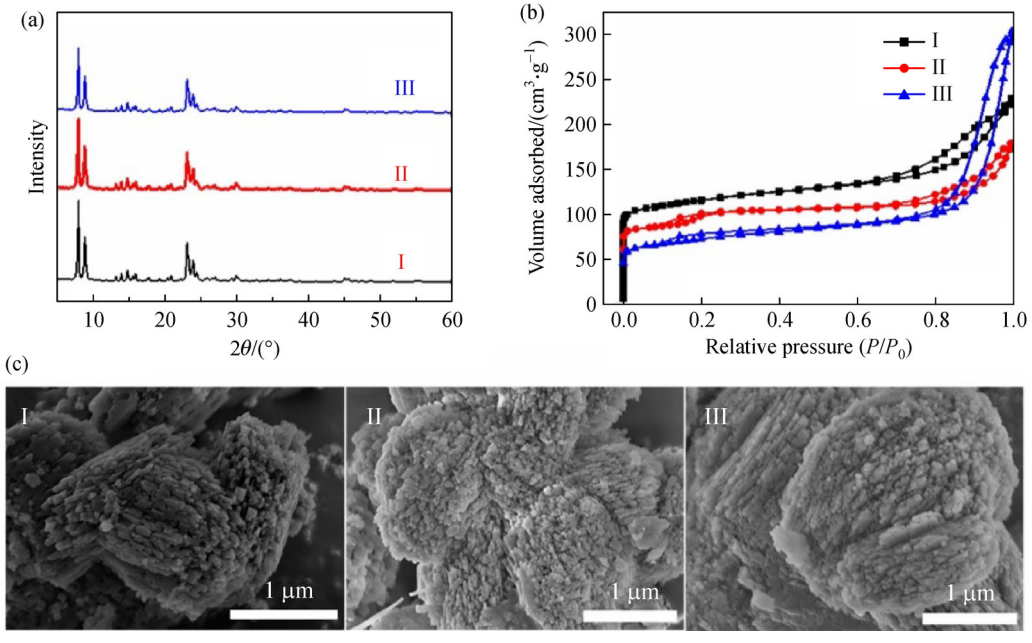


**Fig. 5** (a) XRD patterns; (b) nitrogen adsorption-desorption isotherms; and (c) SEM images of Hier-ZSM-5-100 with different stability tests: (I) crushed with a pressure of 50 MPa; (II) heated at 120 °C for 2 d in Teflon-lined stainless-steel autoclave; (III) treated with steam at 700 °C for 2 h.

destruction of the zeolitic framework. Therein appears a sharp uptake observed at $0.8 < P/P_0 < 1.0$ of the $N_2$ adsorption-desorption isotherms (Fig. 5(b-III), which may be due to the formation of larger mesopores. These mesopores might form at the expense of aluminum extraction, caused by steam treatment at 700 °C, which is referred to as "de-alumination" of zeolite [48–50]. In particular, hierarchical zeolite single crystals are stable after liquid phase hydrothermal treatment. Therefore, hierarchical single-crystal ZSM-5 zeolites are used to catalyze the BA self-etherification reaction, which could ensure that the structure is not destroyed. The Si/Al ratio of all the products was analyzed by ICP characterization (Table 1). The Com-ZSM-5 with a Si/Al ratio of 117 was selected as a reference sample. The XRD pattern (Fig. S9, cf. ESM) and SEM images (Fig. S10, cf. ESM) of Com-ZSM-5 show that the sample has MFI-type characteristic peaks and an uneven size coffin-type morphology. The physicochemical properties of Com-ZSM-5 are shown in Fig. S11 (cf. ESM) and Table 1.

The BA self-etherification reaction was chosen to test the catalytic performance of hierarchical single-crystal ZSM-5 zeolites. The self-etherification reaction was carried out according to the experimental process described by Zhang et al. [40]. Table 1 clearly reveals that the Hier-ZSM-5-100 sample exhibits higher conversion (86.3%) than that of the Com-ZSM-5 samples (64.6%). At the same time, Hier-ZSM-5-100 reveals slightly higher selectivity (96.3%) of product than Com-ZSM-5 (95.8%). The superior performance may be explained by the mesopores introduced in the conventional ZSM-5, which can greatly reduce the diffusion limitation of the reactants. DTBP was then added in another BA self-etherification reaction to poison the active acid sites on the surface of the zeolites and force the catalytic reaction to occur only within the zeolite framework. Note that DTBP is supposed to poison more active sites in hierarchical porous zeolites due to their larger external surface area, leading to decreased conversion of BA. But the conversion of BA (79.8%) and product selectivity (96.0%) shown by Hier-ZSM-5-100 remains greater than that of Com-ZSM-5 with a conversion and selectivity of 57.8% and 93.7%, respectively. This shows that the acid sites in the micropores play a dominant role in hierarchical single-crystal ZSM-5 zeolites. This is further explained by the introduction of mesopores, which greatly reduces the diffusion path, allowing more molecules to diffuse in and out of the pore channels of hierarchical single-crystal zeolites. Further comparisons are also available from Table 1: Hier-ZSM-5-*x* exhibits different conversions of BA of 93.8%, 86.3%, 84.2% and 81.7%, and different selectivities of DBE of 96.1%, 96.3%, 94.2% and 93.8% in a BA self-etherification reaction without DTBP. Likewise, Hier-ZSM-5-*x* in a BA self-etherification reaction containing DTBP exhibits 88.4%, 79.8%, 64.1% and 61.6% conversions of BA and 96.6%, 96.0%, 90.3% and 87.5% selectivity of DBE, respectively. Note that the conversion of BA decreases clearly with increasing Si/Al ratios of Hier-ZSM-5-*x* samples, which is consistent with the change in acidity in Hier-ZSM-5-*x* samples. However, the selectivity of DBE decreases slightly with increasing Si/Al ratios and the S(DBE) and S(DBE)$^{\#}$ of Hier-ZSM-5-*x* ($x$ = 50 and 100) are almost remained the same, which is consistent with the density of micropores in Hier-ZSM-5-*x* samples. It is possible that acidity mainly determines the conversion of BA and that the density of micropores is the key factor for selectivity in the BA self-etherification reaction. Therefore, the introduction of more aluminum in the ZSM-5 framework causes an increase in the defect density in the zeolite framework, which further increases the acidity and the density of micropores present in the zeolite framework. These affect the structure and greatly improve the catalytic performance by tuning conversion and selectivity.

## 4 Conclusions

In this work, we synthesized Hier-ZSM-5-*x* by using ordered mesoporous carbon-silica composite as a hard template. Hierarchical ZSM-5 zeolites are composed of numerous closely packed nanocrystals and nanorods with the same orientation, which forms single zeolite crystals with numerous intracrystalline mesopores. Hierarchical single-crystal ZSM-5 zeolites maintain excellent mechanical and hydrothermal stability. In addition, the introduction of more aluminum into the ZSM-5 framework produces more defects, which generates a large number of micropores and active sites, so the decrease in the Si/Al ratio resulted in significantly increases the acidity and the density of micropores. Furthermore, in the BA self-etherification reaction, hierarchical single-crystal ZSM-5 zeolites offer improved catalytic performance compared with commercial bulk ZSM-5 zeolite. In another study, the external active sites were poisoned by DTBP, but the hierarchical single-crystal ZSM-5 zeolites still presented higher catalytic performance than that of Com-ZSM-5. This can be explained by the introduction of mesopores, which greatly reduce the diffusion path in hierarchical single-crystal ZSM-5 zeolites, thereby allowing guest molecules to easily diffuse in and out of pore channels as compared with Com-ZSM-5. Likewise, the acid sites in the zeolitic framework also play a dominant role in the catalytic performance of hierarchical single-crystal ZSM-5 zeolites. However, the most important result is that the catalytic performance of hierarchical single-crystal ZSM-5 zeolites improves in the BA self-etherification reaction with a decrease in the Si/Al ratio. This is attributed to the increase in micropore density and acidity upon reducing the Si/Al ratio. In summary, the Si/Al ratio in hierarchical single-crystal ZSM-5 zeolites not only determines the pore architecture but also can be used to improve its catalytic

performance by enhancing micropore density and acidity caused by defects in the zeolite framework. Finally, note that this method for preparing hierarchical single-crystal zeolite can be extended to TS-1 zeolite, SAPO-34 zeolite and others.

**Acknowledgements** This work was supported by Innovative Research Team in University (IRT_15R52) of the Chinese Ministry of Education. B.-L. Su acknowledges a Clare Hall Life Membership at the Clare Hall College and the financial support of the Department of Chemistry, University of Cambridge. L.H. Chen acknowledges the Hubei Provincial Department of Education for the "Chutian Scholar" program. This work was also financially supported by the National Natural Science Foundation of China (Grant Nos. 21671155, U1663225, 21805216, 21902122), Major programs of technical innovation in Hubei (No. 2018AAA012) and Hubei Provincial Natural Science Foundation (No. 2018CFA054), Postdoctoral Science Foundation of China (No. 2019M652723).

**Electronic Supplementary Material** Supplementary material is available in the online version of this article at https://doi.org/10.1007/s11705-020-1948-3 and is accessible for authorized users.



## References

1. Aizenberg J, Weaver J C, Thanawala M S, Sundar V C, Morse D E, Fratzl P. Skeleton of *Euplectella* sp.: Structural hierarchy from the nanoscale to the macroscale. Science, 2005, 309(5732): 275–278
2. Sanchez C, Arribart H, Guille M M G. Biomimetism and bioinspiration as tools for the design of innovative materials and systems. Nature Materials, 2005, 4(4): 277–288
3. West G B, Brown J H, Enquist B J. A general model for the origin of allometric scaling laws in biology. Science, 1997, 276(5309): 122–126
4. West G B, Brown J H, Enquist B J. The fourth dimension of life: Fractal geometry and allometric scaling of organisms. Science, 1999, 284(5420): 1677–1679
5. Murray C D. The physiological principle of minimum work: I. the vascular system and the cost of blood volume. Proceedings of the National Academy of Sciences of the United States of America, 1926, 12(3): 207–214
6. Zheng X, Shen G, Wang C, Li Y, Dunphy D, Hasan T, Brinker C J, Su B. Bio-inspired Murray materials for mass transfer and activity. Nature Communications, 2017, 8(1): 14921–14930
7. Shamzhy M, Opanasenko M, Concepcion P, Martinez A. New trends in tailoring active sites in zeolite-based catalysts. Chemical Society Reviews, 2019, 48(4): 1095–1149
8. Tang Y, Li Y, Fung V, Jiang D, Huang W, Zhang S, Iwasawa Y, Sakata T, Luan N, Zhang X, et al. Single rhodium atoms anchored in micropores for efficient transformation of methane under mild conditions. Nature Communications, 2018, 9(1): 1231–1242
9. Peng C, Du Y, Feng X, Hu Y, Fang X. Research and development of hydrocracking catalysts and technologies in China. Frontiers of Chemical Science and Engineering, 2018, 12(4): 867–877
10. Wang N, Sun Q, Bai R, Li X, Guo G, Yu J. *In situ* confinement of ultrasmall Pd clusters within nanosized silicalite-1 zeolite for highly efficient catalysis of hydrogen generation. Journal of the American Chemical Society, 2016, 138(24): 7484–7487
11. Kwok K M, Ong S W D, Chen L, Zeng H C. Transformation of stöber silica spheres to hollow hierarchical single-crystal ZSM-5 zeolites with encapsulated metal nanocatalysts for selective catalysis. ACS Applied Materials & Interfaces, 2019, 11(16): 14774–14785
12. Ennaert T, Van Aelst J, Dijkmans J, De Clercq R, Schutyser W, Dusselier M, Verboekend D, Sels B F. Potential and challenges of zeolite chemistry in the catalytic conversion of biomass. Chemical Society Reviews, 2016, 45(3): 584–611
13. Zhang Q, Chen G, Wang Y, Chen M, Guo G, Shi J, Luo J, Yu J. High-quality single-crystalline MFI-type nanozeolites: A facile synthetic strategy and MTP catalytic studies. Chemistry of Materials, 2018, 30(8): 2750–2758
14. Song B D, Li Y Q, Cao G, Sun Z H, Han X. The effect of doping and steam treatment on the catalytic activities of nano-scale H-ZSM-5 in the methanol to gasoline reaction. Frontiers of Chemical Science and Engineering, 2017, 11(4): 564–574
15. Cychosz K A, Guillet-Nicolas R, Garcia-Martinez J, Thommes M. Recent advances in the textural characterization of hierarchically structured nanoporous materials. Chemical Society Reviews, 2017, 46(2): 389–414
16. Sun M, Chen C, Chen L, Su B. Hierarchically porous materials: Synthesis strategies and emerging applications. Frontiers of Chemical Science and Engineering, 2016, 10(3): 301–347
17. Ding K, Corma A, Maciá Agulló J A, Hu J G, Krämer S, Stair P C, Stucky G D. Constructing hierarchical porous zeolites via kinetic regulation. Journal of the American Chemical Society, 2015, 137(35): 11238–11241
18. Chen L, Li X, Rooke J C, Zhang Y, Yang X, Tang Y, Xiao F, Su B. Hierarchically structured zeolites: Synthesis, mass transport properties and applications. Journal of Materials Chemistry, 2012, 22(34): 17381–17403
19. Zhu J, Meng X, Xiao F. Mesoporous zeolites as efficient catalysts for oil refining and natural gas conversion. Frontiers of Chemical Science and Engineering, 2013, 7(2): 233–248
20. Li S, Li J, Dong M, Fan S, Zhao T, Wang J, Fan W. Strategies to control zeolite particle morphology. Chemical Society Reviews, 2019, 48(3): 885–907
21. Zhang J, Rao C, Peng H, Peng C, Zhang L, Xu X, Liu W, Wang Z, Zhang N, Wang X. Enhanced toluene combustion performance over Pt loaded hierarchical porous MOR zeolite. Chemical Engineering Journal, 2018, 334: 10–18
22. Xu S M, Zhang X X, Cheng D G, Chen F Q, Ren X H. Effect of hierarchical ZSM-5 zeolite crystal size on diffusion and catalytic performance of *n*-heptane cracking. Frontiers of Chemical Science and Engineering, 2018, 12(4): 780–789

23. Xue T, Liu H, Zhang Y, Wu H, Wu P, He M. Synthesis of ZSM-5 with hierarchical porosity: *In-situ* conversion of the mesoporous silica-alumina species to hierarchical zeolite. Microporous and Mesoporous Materials, 2017, 242: 190–199
24. Du S, Sun Q, Wang N, Chen X, Jia M, Yu J. Synthesis of hierarchical TS-1 zeolites with abundant and uniform intracrystalline mesopores and their highly efficient catalytic performance for oxidation desulfurization. Journal of Materials Chemistry. A, Materials for Energy and Sustainability, 2017, 5(17): 7992–7998
25. Fang Y, Yang F, He X, Zhu X. Dealumination and desilication for Al-rich HZSM-5 zeolite via steam-alkaline treatment and its application in methanol aromatization. Frontiers of Chemical Science and Engineering, 2019, 13(3): 543–553
26. Petrov A W, Ferri D, Krumeich F, Nachtegaal M, van Bokhoven J A, Krocher O. Stable complete methane oxidation over palladium based zeolite catalysts. Nature Communications, 2018, 9(1): 2545–2553
27. Pastvova J, Kaucky D, Moravkova J, Rathousky J, Sklenak S, Vorokhta M, Brabec L, Pilar R, Jakubec I, Tabor E, et al. Effect of enhanced accessibility of acid sites in micromesoporous mordenite zeolites on hydroisomerization of *n*-hexane. ACS Catalysis, 2017, 7(9): 5781–5795
28. Li J, Liu M, Guo X, Xu S, Wei Y, Liu Z, Song C. Interconnected hierarchical ZSM-5 with tunable acidity prepared by a dealumination-realumination process: A superior MTP catalyst. ACS Applied Materials & Interfaces, 2017, 9(31): 26096–26106
29. Schwanke A J, Pergher S, Diaz U, Corma A. The influence of swelling agents molecular dimensions on lamellar morphology of MWW-type zeolites active for fructose conversion. Microporous and Mesoporous Materials, 2017, 254: 17–27
30. Wang J, Zhong Z, Ding K, Zhang B, Deng A, Min M, Chen P, Ruan R. Successive desilication and dealumination of HZSM-5 in catalytic conversion of waste cooking oil to produce aromatics. Energy Conversion and Management, 2017, 147: 100–107
31. Wei Z, Xia T, Liu M, Cao Q, Xu Y, Zhu K, Zhu X. Alkaline modification of ZSM-5 catalysts for methanol aromatization: The effect of the alkaline concentration. Frontiers of Chemical Science and Engineering, 2015, 9(4): 450–460
32. Zhang Y, Luo P, Xu H, Han L, Wu P, Sun H, Che S. Hierarchical MFI zeolites with a single-crystalline sponge-like mesostructure. Chemistry (Weinheim an der Bergstrasse, Germany), 2018, 24(72): 19300–19308
33. Shen X, Mao W, Ma Y, Xu D, Wu P, Terasaki O, Han L, Che S. A hierarchical MFI zeolite with a two-dimensional square mesostructure. Angewandte Chemie International Edition, 2018, 130(3): 732–736
34. Soltanali S, Darian J T. Synthesis of mesoporous beta catalysts in the presence of carbon nanostructures as hard templates in MTO process. Microporous and Mesoporous Materials, 2019, 286: 169–175
35. Wang J, Yang M, Shang W, Su X, Hao Q, Chen H, Ma X. Synthesis, characterization and catalytic application of hierarchical SAPO-34 zeolite with three-dimensionally ordered mesoporous-imprinted structure. Microporous and Mesoporous Materials, 2017, 252: 10–16
36. Peng Z, Chen L, Sun M, Zhao H, Wang Z, Li Y, Li L, Zhou J, Liu Z, Su B. A hierarchical zeolitic Murray material with a mass transfer advantage promotes catalytic efficiency improvement. Inorganic Chemistry Frontiers, 2018, 5(11): 2829–2835
37. Di Iorio J R, Gounder R. Controlling the isolation and pairing of aluminum in chabazite zeolites using mixtures of organic and inorganic structure-directing agents. Chemistry of Materials, 2016, 28(7): 2236–2247
38. Locus R, Verboekend D, Zhong R, Houthoofd K, Jaumann T, Oswald S, Giebeler L, Baron G, Sels B F. Enhanced acidity and accessibility in Al-MCM-41 through aluminum activation. Chemistry of Materials, 2016, 28(21): 7731–7743
39. Wang Q, Wang L, Wang H, Li Z, Zhang X, Zhang S, Zhou K. Effect of $SiO_2/Al_2O_3$ ratio on the conversion of methanol to olefins over molecular sieve catalysts. Frontiers of Chemical Science and Engineering, 2011, 5(1): 79–88
40. Zhang X, Liu D, Xu D, Asahina S, Cychosz K A, Agrawal K V, Al Wahedi Y, Bhan A, Al Hashimi S, Terasaki O, et al. Synthesis of self-pillared zeolite nanosheets by repetitive branching. Science, 2012, 336(6089): 1684–1687
41. Li B, Leng K, Zhang Y, Dynes J J, Wang J, Hu Y, Ma D, Shi Z, Zhu L, Zhang D, et al. Metal-organic framework based upon the synergy of a brønsted acid framework and lewis acid centers as a highly efficient heterogeneous catalyst for fixed-bed reactions. Journal of the American Chemical Society, 2015, 137(12): 4243–4248
42. Xu J, Wang Y, Feng W, Lin Y, Wang S. Effect of triethylamine treatment of titanium silicalite-1 on propylene epoxidation. Frontiers of Chemical Science and Engineering, 2014, 8(4): 478–487
43. Tao Y S, Kanoh H, Kaneko K. ZSM-5 monolith of uniform mesoporous channels. Journal of the American Chemical Society, 2003, 125(20): 6044–6045
44. Rhimi B, Mhamdi M, Kalevaru V N, Martin A. Synergy between vanadium and molybdenum in bimetallic ZSM-5 supported catalysts for ethylene ammoxidation. RSC Advances, 2016, 6(70): 65866–65878
45. Fu T, Ma Z, Wang Y, Shao J, Ma Q, Zhang C, Cui L, Li Z. Si/Al ratio induced structure evolution during desilication-recrystallization of silicalite-1 to synthesize nano-ZSM-5 catalyst for MTH reaction. Fuel Processing Technology, 2019, 194: 106–122
46. Haouas M, Taulelle F, Martineau C. Recent advances in application of $^{27}$Al NMR spectroscopy to materials science. Progress in Nuclear Magnetic Resonance Spectroscopy, 2016, 94-95: 11–36
47. Klinowski J. Applications of solid-state NMR for the study of molecular sieves. Analytica Chimica Acta, 1993, 283(3): 929–965
48. Nielsen M, Hafreager A, Brogaard R Y, De Wispelaere K, Falsig H, Beato P, Van Speybroeck V, Svelle S. Collective action of water molecules in zeolite dealumination. Catalysis Science & Technology, 2019, 9(14): 3721–3725
49. Maier S M, Jentys A, Lercher J A. Steaming of zeolite BEA and its effect on acidity: A comparative NMR and IR spectroscopic study. Journal of Physical Chemistry C, 2011, 115(16): 8005–8013
50. Fan Y, Bao X, Lin X, Shi G, Liu H. Acidity adjustment of HZSM-5 zeolites by dealumination and realumination with steaming and citric acid treatments. Journal of Physical Chemistry B, 2006, 110(31): 15411–15416